ELSEVIER

Journal of Magnetism and Magnetic Materials 184 (1998) 127–136

Journal of magnetism and magnetic materials

Structural and magnetic phases of Fe in Fe/Ni(0 0 1) and Fe/$Ni_{81}Fe_{19}$(0 0 1) multilayers

W. Kuch*, S.S.P. Parkin

IBM Research Division, Almaden Research Center, 650 Harry Road, San Jose, CA 95120, USA

Received 30 June 1997; received in revised form 11 December 1997

Abstract

The structure and magnetic properties of ultra-thin Fe spacer layers in epitaxially sputter-deposited Fe/Ni(0 0 1) multilayers are studied using X-ray diffraction and squid magnetometry, and compared to those of similarly deposited Fe/$Ni_{81}Fe_{19}$(0 0 1) multilayers. In both systems, the Fe layers undergo a similar sequence of structural changes with increasing Fe thickness, from a distorted FCC(0 0 1) phase, to a nearly relaxed FCC(0 0 1) phase, to a BCC(0 1 1) phase with concomitant changes in magnetic properties.

PACS: 61.10.− i; 68.65.+g; 75.70.− i

Keywords: Multilayers; X-ray diffraction; Epitaxial growth

1. Introduction

Thin crystalline Fe layers have been extensively studied in recent years because of the subtle interaction between the structure of Fe and its magnetic properties. Ultrathin Fe overlayers deposited on Cu (0 0 1) using thermal or electron-beam evaporation techniques in ultra-high-vacuum chambers form by far the most widely studied system [1–19]. Recently, we have shown that thin Fe layers sandwiched between permalloy ($Ni_{81}Fe_{19}$) layers in sputter-deposited Fe/$Ni_{81}Fe_{19}$(0 0 1) multilayers exhibit similar structures and related magnetic properties, as a function of Fe thickness, as Fe overlayers deposited on Cu(0 0 1) [20]. In this paper we present a detailed study of the structural and magnetic properties of Fe layers in Fe/Ni(0 0 1) multilayers and compare these properties to those of Fe/$Ni_{81}Fe_{19}$(0 0 1) multilayers. We observe only small differences between these two systems, indicating that the Fe properties do not critically depend on the exact nature of the interlayers.

The structure and magnetism of the Fe/Cu(0 0 1) system has been widely studied using a variety of techniques [1–19]. In particular, it has been demonstrated that the FCC phase of Fe is stabilized by growing Fe at room temperature, in a certain

* Corresponding author. On leave from (present address): Max-Planck-Institut für Mikrostrukturphysik, Weinberg 2, D-06120 Halle, Germany. Fax: +49 30 6704 4669; e-mail: kuch@port.exp.bessy.de.

0304-8853/98/$19.00
PII S0304-8853(97)01134-7

thickness range, on Cu(0 0 1) single-crystal substrates [1–6]. Very thin Fe films below the two-dimensional percolation threshold interdiffuse with the substrate even at room temperature, although larger coverages are stable up to higher temperatures [7]. At Fe thicknesses below ≈ 4 monolayers (ML) a vertically expanded FCC-like structure is present [1,2]. Detailed LEED investigations reveal a complicated structure of this phase, with an average interlayer distance of 1.87 Å [1]. In room-temperature grown films, in the thickness range between 4 and 11 ML, a second phase, a relaxed FCC structure, is found [3,4]. LEED analysis of Fe/Cu(0 0 1) in this thickness range reveals flat Fe atomic planes with no vertical (out of plane) distortion except for the topmost layer at the Fe/vacuum interface, which is vertically expanded as for thinner Fe [4]. Structural transitions between these two distinct FCC phases occur not only as a function of Fe thickness, but also as a function of temperature, when the Fe is about 4 ML thick [8]. When the Fe thickness is increased beyond 11 ML, the relaxed Fe fcc phase becomes unstable, and the structure transforms to BCC Fe(0 1 1) [9–12]. Small amounts of BCC precipitates can already be observed at Fe thicknesses as low as 6 ML [11]. The consequence of this transition on magnetic properties, such as magnetic anisotropies, has also been discussed in the literature [13].

Theoretically, it has been predicted that changes in the atomic volume of FCC Fe should result in distinct changes in the Fe magnetic moment. More specifically, the calculations suggest the existence of an antiferromagnetic phase for atomic volumes below 11.9 $Å^3$, and a ferromagnetic phase at higher atomic volumes (> 11.9 $Å^3$) [21]. This has indeed been observed in Fe/Cu(0 0 1), where the vertically expanded phase with an atomic volume of 12.1 $Å^3$ [1] exhibits ferromagnetism [5,6,12], whereas the relaxed phase with only 11.4 $Å^3$ [4] is correlated with an antiferromagnetic phase of Fe [6,14] with a Néel temperature of ≈ 70 K [14]. The BCC phase of Fe, as for the expanded FCC phase, exhibits ferromagnetism [5,6,12].

A similar structural behavior is also observed in Fe films grown on FCC Co(0 0 1) [15–17] and Ni(0 0 1) [16]. A substantial reduction of magnetization of the Fe overlayer in the relaxed FCC phase is also observed in these systems. This seemingly quite general behavior of FCC Fe therefore seems to be dictated mainly by the substrate lattice parameter rather than by the electronic or magnetic properties of the substrate. Indeed, recently, studies of thin Fe layers in [$Fe/Ni_{81}Fe_{19}$] multilayers revealed that the Fe exhibits very similar structural and magnetic properties to that previously observed in ultrathin Fe overlayers [20]. We present in this contribution a detailed structural and magnetic characterization of Fe in epitaxial FCC-(0 0 1) multilayers, prepared by Ar plasma DC-magnetron sputtering. Fe layers, separated either by Nickel or permalloy, exhibit a very similar structural and magnetic behavior, which is very close to that of Fe overlayers on single-crystal substrates. The sequence of the three structural phases observed there, namely the vertically expanded FCC(0 0 1) phase, the relaxed FCC(0 0 1) phase, and also the BCC(0 1 1) phase, are structurally and magnetically characterized in the multilayers, and compared to the respective phases of Fe/Cu(0 0 1).

2. Experiment

The samples were prepared by DC magnetron sputtering from high-purity nickel, permalloy ($Ni_{81}Fe_{19}$), and iron targets. MgO(0 0 1) was used as a substrate, on which Fe and Pt seed layers were grown at a temperature of ≈ 770 K. This enables the subsequent growth of high-quality FCC multilayers. The multilayers were deposited at $T \approx 315$ K and capped with 30 Å Pt. The sample structures are MgO(0 0 1)/Fe(5 Å)/Pt(50 Å)/ [Ni(30 Å)/ $Fe(t_{Fe})]_{11}$/Ni(30 Å)/Pt(30 Å) and MgO(0 0 1)/Fe(5 Å)/ Pt(50 Å)/$[Ni_{81}Fe_{19}(25$ Å$)/Fe(t_{Fe})]_{12}$/Pt(30 Å), where t_{Fe} is the nominal thickness of the Fe layers. The nominal thickness is proportional to the amount of evaporated iron, as taken from the evaporation time. The evaporation rate of the sputter sources is stable within 5%. Using the results of the fit described below, the nominal thickness is calibrated in Å to be identical to the actual thickness for an Fe atomic layer spacing of 1.787 Å and an in-plane density of 1.57×10^{15} atoms/cm^2. Since the lattice parameters of the Fe films depend on the nominal Fe thickness, as will be shown below, the

actual thicknesses of the Fe layers will differ from their nominal thicknesses. For the abscissa of our plots we will use the latter for the sake of simplicity.

The structures of the multilayers were extensively characterized by high-angle X-ray diffraction at ambient pressure and temperature. A Huber four-circle diffractometer with monochromatized Cu K_α radiation was used. In-plane lateral lattice constants were calculated from measured off-specular 2Θ values of the (1 1 1) multilayer diffraction peaks and the specular (0 0 2) peak. The vertical lattice constant was determined from specular diffraction scans around the (0 0 2) reflection. These values were extracted by fitting these data with fitting routines developed by Fullerton [22]. Since the purpose of the fit was just to extract the vertical atomic layer spacings within the layers of the sample, modeling the structure of the multilayers was kept as simple as possible. Neither interdiffusion, nor strain profiles within the individual layers, nor interface roughness was included. Instead, coherent scattering was assumed to be maintained over only a limited number of bilayers. This is a simple means of modeling all types of roughnesses and disorder at the interfaces, including variations in vertical interface atomic distances and interface interdiffusion, and does not imply that the multilayers grow incoherently. Indeed, pseudomorphic growth of the multilayers is found (cf. next section). The multilayers were thus modeled by repeating two independently strained layers with a common in-plane lattice constant. The thicknesses of the nickel and the permalloy layers were determined from a preliminary series of fits and then kept constant for all other samples in a particular series. The only free fitting parameters were the Fe layer thickness, the vertical atomic layer separation within each constituent layer, and the Gaussian width and average number of bilayers which scatter coherently. To account for the scattering from the Pt seed and capping layers, a Lorentzian of order n was additionally fitted to each X-ray scan, where n ranged between 1.6 and 1.8. Further refinements of the model and inclusion of additional fitting parameters, to address, for example, details of the interfaces, did not result in significant changes of the interlayer distances, and thus are not considered here.

Comprehensive magnetic data were obtained in a Quantum Design SQUID magnetometer. Magnetic moment versus field loops were measured for fields ranging between ± 7 T at several temperatures between room temperature and 5 K. The magnetic moment was normalized to the sample area after subtraction of any diamagnetic and/or paramagnetic contributions from the substrate. The substrate contribution was determined from the slope of the moment versus field curve in fields larger than the saturation field of the sample. Thus, the saturation magnetic moment of the sample per unit area was measured as a function of nominal Fe layer thickness at various temperatures. Qualitatively, the data at room temperature were not significantly different from those at 5 K. Thus, magnetic finite-size effects played no important role in our samples. In this paper we include only room temperature SQUID data because this is the temperature at which all our structural data were taken.

3. Results

Fig. 1a shows typical experimental X-ray specular scans and the accompanying fitted curves for $t_{Fe} = 8$ Å for [Fe/Ni] and [Fe/permalloy] (upper and lower curves, respectively). The peaks at a scattering vector $q = 3.2$ Å^{-1} stem from scattering in the Pt seed and capping layers. As can be seen from the figure the scan of Fe/Ni multilayers shows slightly more pronounced bilayer interferences, which are indicative of sharper interfaces, than do the iron/permalloy multilayers. In both cases, however, a good agreement between the model calculations and the experimental curves is evident. The inset shows the rocking curve of the specular (0 0 2) diffraction maximum at $q = 3.52$ Å^{-1} of the $Fe/Ni_{81}Fe_{19}$ multilayer, which exhibits a full-width at half-maximum (FWHM) of 1.3°. Fig. 1b shows an asymmetric azimuthal scan through the (1 1 1) diffraction spots of the $Fe/Ni_{81}Fe_{19}$ multilayer with $t_{Fe} = 8$ Å. An azimuthal angle $\varphi = 0$ corresponds to the FCC [1 0 0] in-plane direction. The fourfold symmetry expected for epitaxial growth is evident. No other peaks than the four sharp (1 1 1) reflections are observed, which each exhibit an FWHM of 1.4°. The inset of Fig. 1b shows the

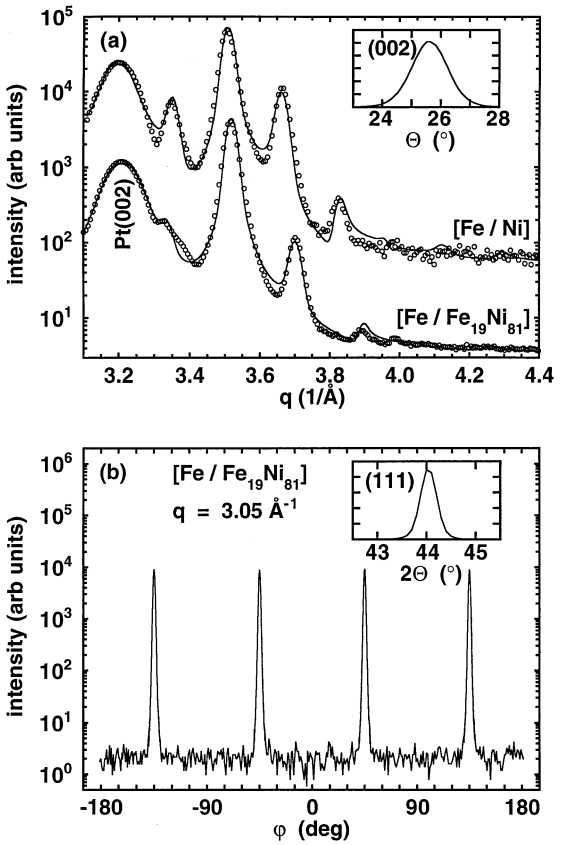

Fig. 1. (a) Specular X-ray diffraction scans around the (0 0 2) diffraction of an [Fe(8 Å)/Ni(30 Å)] (top) and an [Fe(8 Å)/$Ni_{81}Fe_{19}$(25 Å)] multilayer (bottom). The top curve is displaced for clarity. The contributions of the Pt seed and capping layers are indicated. The solid lines represent the results of the fit as described in the text. The inset shows the rocking curve of the specular (0 0 2) diffraction maximum at $q = 3.52\,\text{Å}^{-1}$ of the [Fe(8 Å)/$Ni_{81}Fe_{19}$(25 Å)] multilayer. (b) Asymmetric azimuthal scan through the (1 1 1) diffraction spots of the [Fe(8 Å)/$Ni_{81}Fe_{19}$(25 Å)] multilayer. The inset shows the off-specular Θ–2Θ scan of the (1 1 1) diffraction.

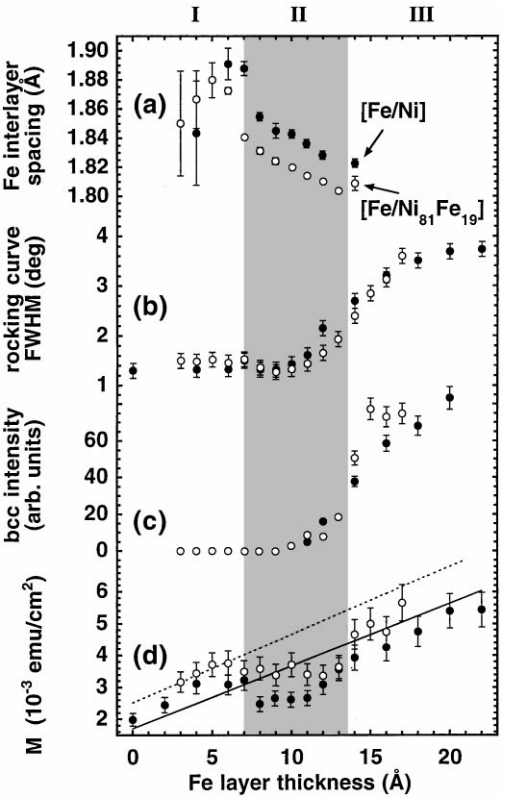

Fig. 2. Structural and magnetic properties of [Fe/Ni] (filled symbols) and [Fe/$Ni_{81}Fe_{19}$] (open symbols) multilayers as a function of nominal Fe layer thickness. (a) average atomic interlayer spacing within the Fe layers; (b) rocking curve full-width at half-maximum (FWHM) of the FCC (0 0 2) multilayer specular diffraction peaks; (c) intensity of the BCC (1 0 1) diffraction peaks; (d) net magnetic moment per unit area of film. Regions I–III denote different structural and magnetic phases of the Fe layers as described in the text.

corresponding off-specular Θ–2Θ scan of the (1 1 1) diffraction. Only a single peak with an FWHM of 0.33° is observed. This demonstrates that the Fe and the $Ni_{81}Fe_{19}$ or Ni layers assume a common in-plane lattice constant, and grow thus pseudomorphically. Summarizing the X-ray diffraction results presented in Fig. 1, the multilayers appear to be of a very high epitaxial quality with respect to epitaxial orientation, mosaic spread, and sharpness of the interfaces. This holds for all Fe/Ni and Fe/$Ni_{81}Fe_{19}$ multilayers for which fits as described in Section 2 were performed [23].

Fig. 2 is a compilation of the results of the structural and magnetic characterization studies. Results for Fe/Ni multilayers are presented and compared to that of Fe/$Ni_{81}Fe_{19}$ multilayers. The data for the two systems are shown as filled and open symbols, respectively. The data for Fe/$Ni_{81}Fe_{19}$ are taken from Ref. [20]. Fig. 2a shows the Fe interlayer spacing d_{Fe} as a function of nominal Fe layer thickness t_{Fe}. At small Fe thicknesses ($t_{Fe} < 4$ Å), at which the Fe layers are

probably too small to develop a well-defined vertical periodicity of their own, or at which the simple modeling of the interfaces is not appropriate, the scattered intensity between two maxima of the specular scans is not completely reproduced in the model calculations. This leads to large error bars in the resulting vertical Fe layer spacing in this thickness regime. At larger thicknesses the simple model yields good agreement with the experimental data. Two distinct iron layer thickness regions can be distinguished with different Fe interlayer spacings: region I at low Fe layer thicknesses with values of d_{Fe} above 1.86 Å (except for the smallest Fe layer thickness of each series), and region II at larger Fe layer thicknesses with smaller interlayer distances which decrease with increasing Fe layer thickness. For Fe/Ni the first region extends to an Fe layer thickness of 7 Å, and for Fe/$Ni_{81}Fe_{19}$ to 6 Å. The corresponding in-plane lattice constants are approximately constant in region I and increase slightly in region II, with the Fe/Ni multilayers having about 0.4% smaller values compared to the Fe/$Ni_{81}Fe_{19}$ multilayers. The iron is tetragonally expanded for all thicknesses in regions I and II. The size of the distortion is significantly higher in the Fe/Ni system with values ranging from 7.1% at $t_{Fe} = 6$ Å in region I, with still large values of 4.8% at $t_{Fe} = 8$ Å, and 2.7% at $t_{Fe} = 14$ Å. In the case of Fe/$Ni_{81}Fe_{19}$ the tetragonal distortion is only 5.9% at $t_{Fe} = 5$ Å, and relaxes from 3.6% at $t_{Fe} = 7$ Å to 1.4% at $t_{Fe} = 13$ Å. We hereby refer to the size of the tetragonal distortion as the ratio of the perpendicular to actual in-plane lattice constants, and not as an expansion with respect to the undistorted equilibrium lattice. The stronger distortion of Fe/Ni as compared to Fe/$Ni_{81}Fe_{19}$ can be rationalized as arising from different strains induced by the nickel and the permalloy layers. The smaller lattice constant of Ni leads to a larger strain on the Fe. Estimating the strain by assuming constant atomic volumes of iron of $t_{Fe} = 13$ Å yields an in-plane strain of -1% for Fe/Ni and -0.5% for Fe/$Ni_{81}Fe_{19}$. The relaxation of the Fe layer distortion in region II may also be qualitatively explained by elastic strain in the multilayers. The iron layers are under compressive strain, whereas the nickel and the permalloy layers are under tensile strain. Increasing the Fe thickness relaxes the strain in the Fe layers, and increases the strain on the nickel or permalloy layers. This leads to the observed change in the vertical lattice constant. The larger thickness of the Ni layers (30 Å) as compared to the $Ni_{81}Fe_{19}$ layers (25 Å) also imposes more elastic stress within the iron/nickel multilayers. This makes the difference in strain induced by the different lattice constants of permalloy and nickel even more pronounced.

The intensity of the FCC diffraction spots is strongly decreased for $t_{Fe} > 14$ Å, and, consequently, it is difficult to fit these data to obtain reliable parameters. Simultaneously, as shown in Fig. 2b, the width of the rocking curves of the (0 0 2) specular diffraction spots increases, which shows that the FCC structure of the films becomes increasingly disordered for thicker Fe layers. As discussed later this is directly correlated to the onset of the formation of BCC Fe. The presence of BCC Fe can be detected by X-ray diffraction, but this is not straightforward because there is no obvious structural relationship between the lattice of BCC Fe and the FCC lattice of Ni or permalloy. To do so, we will explore diffraction from BCC Fe at the (1 0 1) Bragg peak, which, assuming the bulk lattice constant of BCC Fe (2.87 Å), should occur at a scattering vector of $q = 3.10$ Å^{-1}. The angle χ between the [1 0 1] axis and the surface normal is 45° if the BCC Fe is (0 0 1) oriented, and 60° if it is (0 1 1) oriented. At an angle $\chi = 45°$ no diffraction of BCC Fe could be observed at any Fe layer thickness, and thus no ordered (0 0 1) oriented BCC Fe is formed. However, evidence for the formation of (0 1 1)-BCC Fe was found. Scans at an angle $\chi = 60°$, where the azimuthal angle φ is varied, i.e., the sample is rotated about its surface normal, are shown in Fig. 3. The scans were taken for $q = 3.10$ Å^{-1} at Fe/Ni multilayers with Fe layer thicknesses of 10 (open circles) and 18 Å (full circles). Three peaks at azimuthal angles of 28°, 45°, and 62° are observed. The peaks at $\varphi = 28°$ and 62° are identified as contributions from BCC Fe, showing maximum intensity for $q = 3.10$ Å^{-1} and $\chi = 60°$, whereas the peak at $\varphi = 45°$ has its maximum at $q = 3.05$ Å^{-1} and $\chi = 55°$. The latter results from [1 1 1] diffraction of the FCC lattice of the multilayer; as the diffraction spots broaden at larger Fe layer thicknesses, the shoulders of these

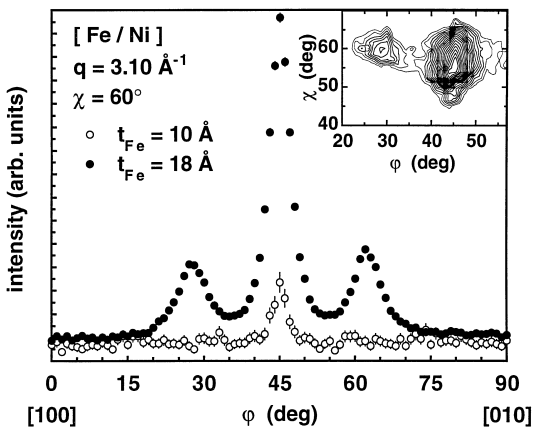

Fig. 3. Azimuthal scans of the diffracted intensity of $[Fe(t_{Fe})/Ni(30\ Å)]_{11}$ multilayers with Fe layer thicknesses $t_{Fe} = 10$ (open circles) and 18 Å (filled circles) at a scattering vector $q = 3.10\ Å^{-1}$, with angle $\chi = 60^\circ$ to the surface normal. The inset shows a contour plot of a two-dimensional scan of both the azimuthal angle φ and χ.

spots become more intense in the X-ray scans as shown in Fig. 3. The situation can be more readily seen in the inset of Fig. 3, which shows a two-dimensional scan of both the azimuthal angle φ and the angle to the surface normal χ. It is clearly seen that the maxima of the two spots are at $\varphi = 45^\circ$, $\chi = 55^\circ$, and at $\varphi = 28^\circ$, $\chi = 60^\circ$, respectively.

The BCC diffraction spots at $\varphi = 28^\circ$ and 62° are first observed at Fe layer thicknesses around 11 Å, and increase in intensity with increasing Fe layer thickness. Plots of the intensity of these spots versus Fe layer thickness for both [Fe/Ni] and $[Fe/Ni_{81}Fe_{19}]$ are given in Fig. 2c. It is clear for both multilayer systems that the width of the FCC diffraction spots (Fig. 2b) parallel the increase in intensity of the BCC diffraction peaks. We thus may conclude that the decrease in FCC epitaxial quality of the multilayers is correlated with the appearance of BCC Fe.

The structural changes of the multilayers with varying Fe thickness are directly reflected in their magnetic properties. The room temperature magnetic moment per unit area of the multilayers is summarized in Fig. 2d as a function of the nominal Fe layer thickness. For small Fe thicknesses, in region I, the moments increase approximately linearly with t_{Fe}, consistent with uniformly magnetized Fe layers. Indeed, in region I, the moments of the multilayers can be well described using bulk magnetic moments of the magnetic metals. Calculated moments for Fe/Ni and $Fe/Ni_{81}Fe_{19}$ multilayers, respectively, using bulk magnetic moments of iron, nickel, and permalloy from Ref. [24] are shown as solid and dotted lines in Fig. 2d. By contrast, in region II the experimentally measured moments no longer vary linearly with Fe thickness (see shaded region in Fig. 2). The magnetic moment of the multilayers actually decreases with increasing Fe thickness, reaching a minimum at about 11–12 Å Fe layer thickness with a moment comparable to that at $t_{Fe} \approx 3$ Å. Thus, in region II much of the Fe contributes no net magnetic moment. In Fig. 4 we show magnetic moment versus field curves for $Fe/Ni_{81}Fe_{19}$ multilayers representative of region I ($t_{Fe} = 5$ Å, solid symbols) and region II ($t_{Fe} = 9$ Å, open symbols). The curve for $t_{Fe} = 5$ Å exhibits relatively small saturation fields and a square shape characteristic of a ferromagnetic response of the system. This is in accordance with an entirely magnetic structure in region I. For $t_{Fe} = 9$ Å a tilted loop with high saturation fields is observed. The saturation magnetic moment per unit area of this sample is lower than that of the multilayer with 5 Å Fe layers, although the anticipated moment based on the amount of Fe in the sample is higher (cf. Fig. 2d). The tilted magnetization loop in region II further supports the picture of Fe exhibiting no net magnetic moment: An antiferromagnetic coupling of the permalloy layers (and probably also of some of the interfacial Fe) over the non-ferromagnetic Fe can explain the observed magnetization curve. This is indeed confirmed by the observation of giant magnetoresistance, which in this sample amounts to about 4% [25].

In region III, the magnetic moment of the multilayers again strongly increases with increasing Fe thickness, approaching the calculated moments at the highest Fe layer thicknesses under investigation. This is attributed to the formation of BCC Fe, which, in contrast to the Fe of region II, shows ferromagnetic behavior. The slope of the curve of the experimental magnetic moment versus t_{Fe} between $t_{Fe} = 12$ and 15 Å is higher than the calculated slope. If we correlate the increase in

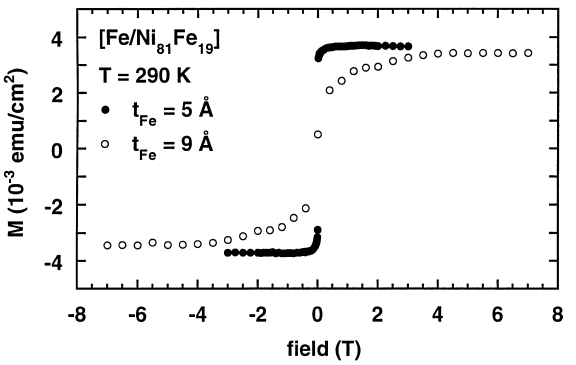

Fig. 4. Magnetic moment versus field curves for $[Fe(t_{Fe})/Ni_{81}Fe_{19}(25\ Å)]_{12}$ multilayers with Fe layer thicknesses $t_{Fe} = 5$ (filled circles) and 9 Å (open circles).

moment in region III to the presence of BCC Fe, this confirms that a transformation of FCC material into BCC occurs when the Fe layer thickness is increased.

4. Discussion

The presence of two distinct FCC phases of Fe with different tetragonal expansions (regions I and II) closely resembles the structural behavior found in Fe/Cu(0 0 1). In the latter case, for thicknesses up to 4 ML a structural phase with a strongly vertically expanded Fe–Fe interlayer distance is found. In Fe/Cu(0 0 1) detailed LEED investigations have revealed a complicated structure involving sinusoidal shifting and vertical buckling of the entire Fe film [1]. The average interlayer distance was found to be 1.87 Å, with substantial variation in the interlayer spacing of the individual Fe layers [1]. We find very similar Fe interlayer spacings in $Fe/Ni_{81}Fe_{19}$ multilayers over the same Fe thickness range (cf. Fig. 2a and Fig. 2e). The Fe layers in Fe/Ni are under higher strain than the Fe layers in $Fe/Ni_{81}Fe_{19}$, because of the smaller lattice constant of Nickel compared to permalloy, and because of the larger thickness of the Ni layers in our samples. This leads to the observed difference in d_{Fe}. On the contrary, although, in principal, the Fe layers in both Fe/Ni and in $Fe/Ni_{81}Fe_{19}$ are more strongly strained than Fe on Cu(0 0 1), this does not seem to be reflected in the vertical lattice constants. A much smaller distortion is observed than is expected, and the expansion of the atomic volume in region I of Fe in the multilayers is actually slightly smaller than in Fe/Cu(0 0 1). Whereas in Fe/Cu(0 0 1) an atomic volume of 12.1 $Å^3$ was obtained from a LEED analysis [1], the atomic volume of Fe in the multilayers attains only 11.8 $Å^3$ for both [Fe/Ni] and $[Fe/Ni_{81}Fe_{19}]$ in region I. Despite this difference in atomic volume, it is evident that the strong vertical expansion of Fe in the multilayers is similar to that found in Fe/Cu(0 0 1). Furthermore, the poorer agreement with the simple structural model used for the fits in region I compared to region II could possibly be accounted for by a complex reconstruction within the Fe layers perhaps similar to that described in Ref. [1]. These authors find a systematic variation of the Fe interlayer spacing away from the Cu(0 0 1) substrate. Such a systematic variation would lead to a failure of the model used to fit the X-ray data. In summary, despite the different environment of the Fe layers in the multilayers and Fe/Cu(0 0 1), there is a striking similarity in their structure in region I.

In region II, the simple model used for the fits agrees well with experiment, which indicates a simpler structure for the Fe layers. Taken together with the smaller distortion compared to region I, the Fe structure is a more relaxed FCC structure similar to that found for Fe films on Cu(0 0 1) at thicknesses between 4 and 11 ML. LEED analysis of Fe/Cu(0 0 1) in this thickness range of the relaxed FCC phase of Fe reveals flat Fe atomic planes with no vertical distortion except for the topmost layer at the Fe/vacuum interface, which remains vertically expanded [4]. Again, we conclude that the same structural behavior is found in the multilayers, with the residual vertical expansion of the Fe layers being due to elastic strain induced by the nickel or permalloy layers.

The finding of non-ferromagnetic iron in region II parallels the magnetic behavior observed for the relaxed FCC phase in Fe/Cu(0 0 1). Kerr measurements have shown that in that system the average Fe magnetic moment of the relaxed FCC phase is strongly reduced [5,6,18]. As explained in Section 1, this is attributed to an antiferromagnetic phase of Fe [6,14], correlated to the structural

phase via the atomic volume [21]. A similar magnetic behavior of thin Fe films was also observed on Ni(0 0 1) and FCC Co(0 0 1) substrates [15–17]. The atomic volume of the relaxed FCC phase in Fe/Cu(0 0 1) has been determined by LEED analysis as 11.4 Å^3 [4]. The atomic volume of Fe in region II of the multilayers decreases from 11.6 Å^3 at $t_{Fe} = 8$ Å to 11.4 Å^3 at $t_{Fe} = 13$ Å, with similar values for both [Fe/Ni] and [Fe/$Ni_{81}Fe_{19}$]. The Fe layers thus tend to adopt the same atomic volume as in the relaxed FCC phase of Fe/Cu(0 0 1) when the compressive strain from the sandwiching nickel and permalloy layers is relieved. We conclude that the reason for the reduced magnetic moment in region II, as in Fe/Cu(0 0 1), is the dependence of the magnetic phase of FCC Fe on the lattice constant, as outlined in Ref. [21].

An alternative explanation to account for the reduced moment in Fe is the possibility of a complicated magnetic domain structure in which the Fe layer breaks up into very small ferromagnetic regions [19]. We can rule this out because of the large magnetic fields in which we measured the saturation magnetization, the absence of any significant temperature effect, and the observation of antiferromagnetic behavior as well as GMR.

We will now focus on the third structural region, region III, beginning at $t_{Fe} = 14$ Å. This region is characterized by reduced X-ray scattering intensity, a substantial broadening of the FCC diffraction spots, and increasing scattering signal from BCC Fe. From X-ray diffraction we see that the BCC Fe is (0 1 1) oriented. The same orientation of BCC Fe was found in Fe/Cu(0 0 1) for Fe thicknesses above 10–11 ML [5,9,10]. Our X-ray diffraction data show that the azimuthal orientation of the BCC-[1 0 1] axis is rotated by 28° ± 0.2° with respect to the [1 0 0] axis of the FCC material. The BCC-[0 1 1] axis is thus aligned along the FCC-[0 0 1] axis, and rotated such that the angle between the projection of the BCC-[1 0 1] axis onto the surface plane, which is the BCC-[2 $\bar{1}$ 1] axis in our case, has an angle of 28° with the FCC-[1 0 0] axis. This is shown schematically in Fig. 5, where these two directions are indicated by arrows in the bottom. Due to the fourfold symmetry of the substrate there are four equivalent domains of BCC orientation, resulting in eight BCC peaks in a complete azimuthal scan at angles of (0°, 90°, 180°, 270°) ± 28°. In Fe/Cu(0 0 1), the BCC Fe was found to be oriented with its [1 $\bar{1}$ 1] axis along the FCC-[1 1 0] axis [10], from which one calculates an angle of 25.5° between [2 $\bar{1}$ 1]$_{BCC}$ and [1 0 0]$_{FCC}$. In Fig. 5 this would correspond to the alignment of the densely packed [2 1 $\bar{1}$] rows of the BCC material (horizontal in Fig. 5) along the FCC-[1 $\bar{1}$ 0] direction. The BCC Fe in the multilayers thus exhibits a very similar, yet not identical azimuthal orientation as that in Fe/Cu(0 0 1). Since it is likely that the orientation of the BCC Fe phase can be more reliably determined from X-ray studies, the different orientation we find in the multilayers as compared to prior work on Fe/Cu(0 0 1) may not be significant. However, one could postulate that this difference in the azimuthal orientation, if significant, might result from the different lattice constants of Cu and Ni or $Ni_{81}Fe_{19}$, respectively. The smaller lattice constant of nickel or permalloy as compared to copper suggests that a possible match between the [3 $\bar{1}$ 1] axis of the BCC Fe and the FCC-[3 1 0] axis might also become important. An alignment of [3 $\bar{1}$ 1]$_{BCC}$ and [3 1 0]$_{FCC}$ is equivalent

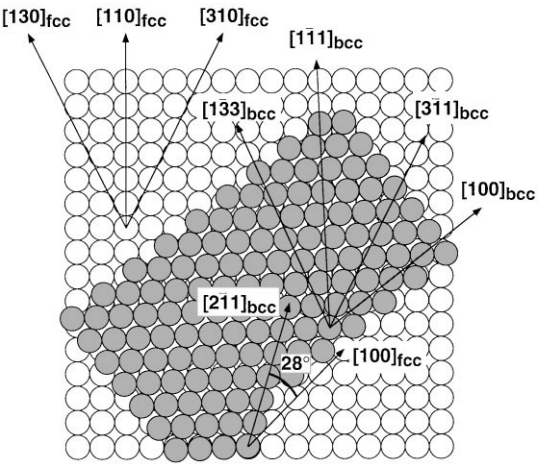

Fig. 5. Schematic illustration of the orientation of BCC Fe with respect to an FCC underlayer. The BCC-[2 $\bar{1}$ 1] axis is rotated by 28° with respect to the [1 0 0]$_{FCC}$ axis, as depicted. Other crystallographic directions which are discussed in the text are also explained by arrows. Note that due to the fourfold symmetry of the FCC layer there are four equivalent orientations of the BCC material.

to an angle of 28.5° between $[2\,\bar{1}\,1]_{BCC}$ and $[1\,0\,0]_{FCC}$, which is very close to the observed 28°. An alignment of $[1\,\bar{3}\,3]_{BCC}$ and $[1\,3\,0]_{FCC}$ ($\varphi = 28.5°$) could also help to turn the azimuthal orientation from 25.5° to 28°. To illustrate this, these directions are marked by arrows in Fig. 5. There is, however, a considerable mismatch between the nearest neighbor distance in the $[3\,\bar{1}\,1]$ direction of BCC Fe and the FCC-[3 1 0] direction of about -14% for Ni and -15% for permalloy. Between $[1\,\bar{3}\,3]_{BCC}$ and 130_{FCC} the mismatch is $+12\%$ for Ni and $+11\%$ for permalloy. Perhaps the explanation for the actual in-plane orientation can only be determined from a precise calculation of the energetically most favorable configuration of this system. Such a calculation would have to account for the complicated transformation of FCC to BCC and the simultaneous presence of both FCC Fe and BCC Fe in a certain thickness range [11,12].

It cannot be completely excluded that a portion of the nickel or permalloy layers are transformed into BCC. Ni has been found to grow as BCC Ni for small thicknesses on BCC Fe(0 0 1) [26]. In our case, X-ray diffraction detected no other BCC signal than that corresponding to a scattering vector consistent with the lattice constant of unstrained bulk BCC Fe. Since the atomic density of Ni is different from that of iron, and thus should lead to a different scattering vector, this is a strong indication that the observed scattering is indeed mainly due to bcc Fe and not to BCC Ni. We, however, cannot rule out the possibility that unordered BCC Ni or permalloy might be formed when deposited onto the BCC Fe layers. If this were the case, it most probably would also affect the azimuthal orientation of the BCC Fe.

5. Conclusions

In summary, detailed studies of the structure of thin Fe layers in (0 0 1) Fe/Ni and Fe/permalloy multilayers show that the Fe layers in each case exhibit three distinct structural types. As the Fe layer thickness is increased its structure varies from a vertically expanded FCC structure to a nearly relaxed FCC phase, and finally to a BCC(0 1 1) phase. These phases are almost identical to those found in thin Fe layers grown on Cu(0 0 1) single crystals. Although the nearly relaxed FCC phase in the multilayers is significantly distorted as compared to the almost pure FCC structure of the corresponding phase in Fe/Cu(0 0 1), the unusual magnetic properties of this phase in Fe/Cu(0 0 1) are also found in the multilayers. In particular, in both cases, the net magnetic moment of the Fe atoms in this phase is substantially reduced. The residual distortion of this phase in the multilayers is attributed to elastic strain. The third structural phase of Fe in Fe/Cu(0 0 1), BCC Fe(0 1 1), is to within 3° of azimuthal orientation identically reproduced in the multilayers. Altogether, the structure and corresponding magnetic behavior of thin Fe layers in Fe/Ni and $Fe/Ni_{81}Fe_{19}$ multilayers is qualitatively identical to that found previously in ultrathin Fe films on Cu(0 0 1). We conclude that Fe in FCC-(0 0 1) multilayers is an excellent example where knowledge acquired from studies of single crystalline overlayers can be applied to more complicated structures grown by very different techniques.

Acknowledgements

We thank M.F. Toney for fruitful discussions, and K.P. Roche for his technical expertise. S.S.P.P. thanks the Office of Naval Research for partial support of this work.

References

[1] S. Müller, P. Bayer, C. Reischl, K. Heinz, B. Feldmann, H. Zillgen, and M. Wuttig, Phys. Rev. Lett. 74 (1995) 765; S. Müller, P. Bayer, A. Kinne, C. Reischl, R. Metzler, K. Heinz, Surf. Sci. 331–333 (1995) 723; K. Heinz, S. Müller, P. Bayer, Surf. Sci. 337 (1995) 215.

[2] M.T. Kief, W.F. Egelhoff Jr., Phys. Rev. B 47 (1993) 10 785; J.V. Barth, D.E. Fowler, Phys. Rev. B 52 (1995) 11 432.

[3] S.H.Lu, J. Quinn, D. Tian, F. Jona, P.M. Marcus, Surf. Sci. 209 (1989) 364; M. Wuttig, J. Thomassen, Surf. Sci. 282 (1993) 237; J.V. Barth, D.E. Fowler, Phys. Rev. B 52 (1995) 1528.

[4] P. Bayer, S. Müller, P. Schmailzl, K. Heinz, Phys. Rev. B 48 (1993) 17 611; S. Müller, P. Bayer, A. Kinne, P. Schmailzl, K. Heinz, Surf. Sci. 322 (1995) 21.

[5] J. Thomassen, F. May, B. Feldmann, M. Wuttig, H. Ibach, Phys. Rev. Lett. 69 (1992) 3831.
[6] D. Li, M. Freitag, J. Pearson, Z.Q. Qiu, S.D. Bader, Phys. Rev. Lett. 72 (1994) 3112; J. Appl. Phys. 76 (1994) 6425; S.D. Bader, D. Li, J. Magn. Magn. Mater. 156 (1996) 153.
[7] T. Detzel, N. Memmel, Phys. Rev. B 49 (1994) 5599.
[8] M. Zharnikov, A. Dittschar, W. Kuch, C.M. Schneider, J. Kirschner, Phys. Rev. Lett. 76 (1996) 4620; J. Magn. Magn. Mater. 174 (1997) 40.
[9] M. Wuttig, B. Feldmann, J. Thomassen, F. May, H. Zillgen, A. Brodde, H. Hannemann, H. Neddermayer, Surf. Sci. 291 (1993) 14; T. Detzel, N. Memmel, T. Fauster, Surf. Sci. 293 (1993) 227; N. Memmel, T. Detzel, Surf. Sci. 307–309 (1994) 490.
[10] P. Schmailzl, K. Schmidt, P. Bayer, R. Döll, K. Heinz, Surf. Sci. 312 (1994) 73.
[11] J. Giergiel, J. Kirschner, J. Landgraf, J. Shen, J. Woltersdorf, Surf. Sci. 310 (1994) 1.
[12] J. Giergiel, J. Shen, J. Woltersdorf, A. Kirilyuk, J. Kirschner, Phys. Rev. B 52 (1995) 8528.
[13] M. Wuttig, B. Feldmann, T. Flores, Surf. Sci. 331–333 (1995) 659; D.E. Fowler, J.V. Barth, Phys. Rev. B 53 (1996) 5563.
[14] R.D. Ellerbrock, A. Fuest, A. Schatz, W. Keune, R.A. Brand, Phys. Rev. Lett. 74 (1995) 3053.
[15] W.L. O'Brien, B.P. Tonner, Surf. Sci. 334 (1995) 10.
[16] W.L. O'Brien, B.P. Tonner, Phys. Rev. B 52 (1995) 15 332; J. Appl. Phys. 79 (1996) 5629.
[17] E.J. Escorcia-Aparicio, R.K. Kawakami, Z.Q. Qiu, Phys. Rev. B 54 (1996) 4155; J. Appl. Phys. 79 (1996) 4964; R.K. Kawakami, E.J. Escorcia-Aparicio, Z.Q. Qiu, J. Appl. Phys. 79 (1996) 4532.
[18] W.A.A. Macedo, W. Keune, E.D. Ellerbrock, J. Magn. Magn. Mater. 93 (1991) 552; T. Detzel, M. Vonbank, M. Donath, V. Dose, J. Magn. Magn. Mater. 147 (1995) L1.
[19] R. Allenspach, A. Bischof, Phys. Rev. Lett. 69 (1992) 3385.
[20] W. Kuch, S.S.P. Parkin, Europhys. Lett. 37 (1997) 465.
[21] V.L. Moruzzi, P.M. Marcus, K. Schwartz, P. Mohn, Phys. Rev. B 34 (1986) 1784; V.L. Moruzzi, P.M. Marcus, J. Kübler, Phys. Rev. B 39 (1989) 6957.
[22] E.E. Fullerton, I.K. Schuller, H. Vanderstraeten, Y. Bruynseraede, Phys. Rev. B 45 (1992) 9292.
[23] The epitaxial parameters of our Fe/Ni and Fe/$Ni_{81}Fe_{19}$ multilayer samples are, for example, only slightly inferior to those of sputtered Fe/Cr multilayers, for which an epitaxial quality similar to that of molecular beam epitaxy grown films has been stated (E.E. Fullerton, M.J. Conover, J.E. Mattson, C.H. Sowers, S.D. Bader, Phys. Rev. B 48 (1993) 15 755).
[24] B.D. Cullity, Introduction to Magnetic Materials, Addison-Wesley, Reading, MA, 1972.
[25] S.S.P. Parkin et al., in preparation.
[26] Z.Q. Wang, Y.S. Li, F. Jona, P.M. Marcus, Solid State Commun. 61 (1987) 623; B. Heinrich, S.T. Purcell, J.R. Dutcher, K.B. Urquhart, J.F. Cochran, A.S. Arrott, Phys. Rev. B 38 (1988) 12 879.